

Magnetic-anisotropy induced spin blockade in a single-molecule transistor

Guangpu Luo and Kyungwha Park*

Department of Physics, Virginia Tech, Blacksburg, Virginia 24061, USA

(Dated: September 20, 2016)

We present a new mechanism for a spin blockade effect associated with a change in the type of magnetic anisotropy over oxidation state in a single molecule transistor, by taking an example of an individual $\text{Eu}_2(\text{C}_8\text{H}_8)_3$ molecule weakly coupled to non-magnetic electrodes without linker groups. The molecule switches its magnetization direction from in-plane to out-of-plane when it is charged. In other words, the magnetic anisotropy of the molecule changes from easy plane to easy axis when the molecule is charged. By solving the master equation based on model Hamiltonian, we find that current through the molecule is highly suppressed at low bias independently of gate voltage due to the interplay between spin selection rules and the change in the type of magnetic anisotropy. Transitions between the lowest magnetic levels in successive charge states are forbidden because the magnetic levels differ by $|\Delta M| > 1/2$ due to the change in the type of magnetic anisotropy, although the total spins differ by $|\Delta S| = 1/2$. This current suppression can be lifted by significant \mathbf{B} field, and the threshold \mathbf{B} field varies as a function of the field direction and the strength of magnetic anisotropy. The spin blockade effect shed light on switching the magnetization direction by non-spin-polarized current and on exploring effects of this property coupled to other molecular degrees of freedom.

PACS numbers: 73.23.Hk, 75.50.Xx, 73.63.-b

I. INTRODUCTION

Individual nanoscale molecules have been successfully bridged between electrodes within single-molecule transistors or scanning tunneling microscopy in the laboratory. In particular, studies of electron tunneling through individual *anisotropic* magnetic molecules showed unusual properties ranging from nuclear spin states controlled by electric field¹, Berry-phase oscillations of the Kondo peaks², spin-polarized current induced magnetic switching^{3,4}, complete current suppression⁵, large spin filtering⁶, and giant molecular magnetocapacitance⁷. In these cases, magnetic anisotropy induced by spin-orbit coupling and Jahn-Teller distortion plays a crucial role.

Within a magnetic molecule or system, it is difficult to switch the *type* of magnetic anisotropy (i.e., easy axis or easy plane) or the *sign* of the magnetic anisotropy parameter with oxidation state or via charge transfer (from a non-magnetic substrate) because the anisotropy type is often determined by the shape or orientation of the molecule. Instead, the magnitude of the magnetic anisotropy parameter or the type of magnetic ordering can be relatively easily varied^{5,8-12}. A change in oxidation state or charge transfer rarely alters orbital character critical to the anisotropy¹⁰⁻¹². However, there are some exceptional cases¹³⁻¹⁵. First-principles-based calculations revealed that an Eu-sandwiched triple-decker molecule, $\text{Eu}_2(\text{COT})_3$ ($\text{COT}=\text{C}_8\text{H}_8$), switches its magnetization direction from in-plane (xy plane) to out-of-plane (along the z axis) when it is charged¹³ [Fig. 1(a)-(c)]. Fe-based molecules (on copper)¹⁴ and cobalt films¹⁵ were shown to change their magnetization directions from in-plane to out-of-plane by oxygen adsorption onto the molecules and by coating the films with graphene, respectively.

In this work we present a new mechanism for a spin blockade effect associated with a change in the *type* of magnetic anisotropy or in the *sign* of the magnetic anisotropy parameter in a single molecule transistor, by taking an example of a single $\text{Eu}_2(\text{COT})_3$ molecule weakly coupled to non-magnetic electrodes. $\text{Eu}_n(\text{COT})_{n+1}$ clusters ($n = 1, 2, \dots, 18$) have been synthesized and their magnetic properties have been characterized^{16,17}. Similar lanthanide-based anisotropic molecules, $[\text{Ln}_n(\text{COT}')_{n+1}]$, were synthesized in crystal phases and they were also formed in solutions¹⁸⁻²⁰. By solving the master equation, we find that electron transport via the molecule shows Coulomb blockade-like behavior with one unique feature: current is highly suppressed at low bias independently of gate voltage. This suppression is caused by the interplay between spin selection rules and the sign reversal of the magnetic anisotropy parameter. The lowest magnetic levels in successive charge states differ by greater than $1/2$, $|\Delta M| > 1/2$, although the total spins differ by $1/2$, due to the sign change in the magnetic anisotropy parameter [Fig. 1(b), (c), and (e)]. Thus, the spin selection rules prevent transitions between the lowest magnetic levels at zero bias. This spin blockade effect can be lifted by significant \mathbf{B} field, and the threshold \mathbf{B} field depends on the field direction and the magnetic anisotropy parameter.

To the best of our knowledge, this kind of a spin blockade effect has not been studied before and it is distinct from other (spin) blockade effects. A spin blockade effect was reported in quantum dots when the total spins of successive charge states differ by greater than $1/2$ ($|\Delta S| > 1/2$) due to the spin selection rules²¹ [Fig. 1(d)]. Pauli spin blockade was observed when tunneling between singlet and triplet states is forbidden due to the Pauli exclusion principle in coupled quantum dots^{22,23}. Franck-Condon blockade occurs when vibron-assisted

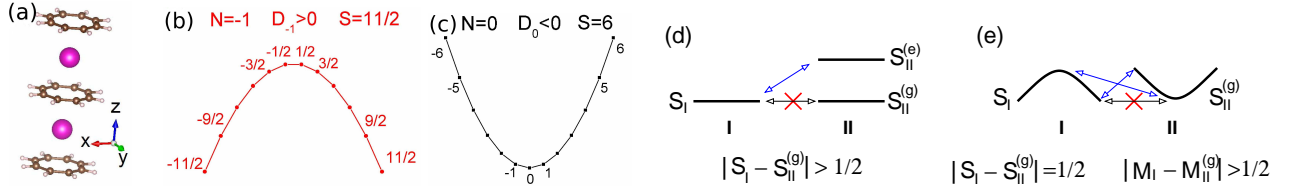


FIG. 1: (Color online) (a) Geometry of $\text{Eu}_2(\text{COT})_3$. (b)-(c) Easy-axis and easy-plane magnetic anisotropy for the cationic ($N = -1$) and neutral ($N = 0$) states of $\text{Eu}_2(\text{COT})_3$, respectively, where $D_{-1,0}$ are the magnetic anisotropy parameters and S is the total spin of the molecule. Magnetic levels M are shown for a given total spin S , where the M values are eigenvalues of the z component of the total spin operator. (d) Spin blockade mechanism in Ref.21, where S_I , $S_{II}^{(g)}$, and $S_{II}^{(e)}$ are the total spins of charge state I and ground-state and excited-state of charge state II, respectively. For a given total spin, different M levels are all degenerate due to the absence of magnetic anisotropy. (e) Spin blockade mechanism in this work. In (d) and (e), the total numbers of electrons in successive charge states I and II differ by unity: $|N_I - N_{II}| = 1$. Forbidden transitions are shown with red “X” marks, while allowed transitions are shown with blue arrows. For details, see the text.

electron tunneling dominates due to strong electron-vibron coupling^{24,25}. The blockade effect observed in Ref.5 arises from low-lying spin multiplets. Our concept and results are quite general and so they can be applied to any anisotropic molecules in which the type of magnetic anisotropy can be switched over oxidation state or charge transfer. The spin blockade effect we report may shed light on controlling the magnetization direction by non-spin-polarized current without \mathbf{B} field, as well as on exploring effects of this unique property coupled to other molecular degrees of freedom on electron and thermal transport.

II. THEORETICAL MODEL

In our model, we assume that an individual $\text{Eu}_2(\text{COT})_3$ molecule is bridged between non-magnetic metallic electrodes without linker groups (i.e., no chemical bonding) and that the molecule can be in a cationic ($N = -1$) or neutral ($N = 0$) state by varying gate voltage V_g . We consider only two charge states of the molecule because transport experiments on anisotropic magnetic molecules often reveal only two charge states^{9,26,27} and because the charging energies of anisotropic magnetic molecules are typically several eV^{6,28}. Figure 3 in Ref. [13] showed that with spin orbit coupling, the highest occupied molecular orbital (HOMO) level is split into two singly occupied levels, levels 3 and 4, where level 3 has a higher energy than level 4. We assume that the $\text{Eu}_2(\text{COT})_3$ molecule is positively ionized such that the zero-bias Fermi levels of the electrodes are located between level 3 and level 4. The molecular orbital level for the $N = -1$ ($N = 0$) state corresponds to level 4 (level 3). We set the orbital energies of $N = -1$ and $N = 0$ as zero and ε , respectively. For $N = -1$, the molecule has the total spin $S = 11/2$ with out-of-plane magnetic anisotropy (z axis)¹³ [Fig. 1(b)]. The z axis is normal to the plane where (COT)₃ lie, as shown in Fig. 1(a). For $N = 0$, the total spin becomes $S = 6$, and the magnetization direction switches to easy plane (xy plane)¹³ [Fig. 1(c)]. The molecular Hamiltonian,

\mathcal{H}_{mol} , (adapted from Refs.3,24,29,30) reads

$$\mathcal{H}_{\text{mol}} = -D_N (S_z^{(N)})^2 + (\varepsilon - eV_g) \sum_{\sigma} c_{\sigma}^{\dagger} c_{\sigma} + g\mu_B \mathbf{S}^{(N)} \cdot \mathbf{B}, \quad (1)$$

where D_N is a magnetic anisotropy parameter for state N with spin $S^{(N)}$. We use $D_{N=-1} = 0.0637$ meV for $S^{(N=-1)}=11/2$ and $D_{N=0}=-0.0744$ meV for $S^{(N=0)}=6$ (Ref. 13). We neglect transverse magnetic anisotropy since it is typically much smaller than the $|D_N|$ value. The second term in \mathcal{H}_{mol} describes an electron with spin σ tunneled to the molecular orbital ε . In our calculations, for convenience, the value of ε is included in the value of V_g . Here c_{σ}^{\dagger} and c_{σ} are electron creation and annihilation operators. The last term is the Zeeman energy with $g = 2$. Main differences between our model and model Hamiltonian in Refs.3,29,30 are as follows: in the latter, (i) three charge states ($N = 0, 1, 2$) were considered with on-site Coulomb repulsion which is needed due to double occupancy at the lowest unoccupied molecular orbital (LUMO); (ii) at least one of the electrodes was ferromagnetic; (iii) the sign of the magnetic anisotropy parameter remained the same for different charge states.

The Hamiltonian $\mathcal{H}_{\text{el}} = \sum_{\alpha=L,R} \sum_{\mathbf{k},\sigma} \epsilon_{\mathbf{k},\sigma}^{\alpha} a_{\mathbf{k},\sigma}^{\alpha\dagger} a_{\mathbf{k},\sigma}^{\alpha}$ is for the non-magnetic metallic electrodes, where $a_{\mathbf{k},\sigma}^{\alpha\dagger}$ and $a_{\mathbf{k},\sigma}^{\alpha}$ are creation and annihilation operators for an electron at electrode α with energy $\epsilon_{\mathbf{k},\sigma}^{\alpha}$, momentum \mathbf{k} and spin σ . The Hamiltonian for the tunneling between the electrodes α and the molecule is

$$\mathcal{H}_{\text{T}} = \sum_{\alpha=L,R} \sum_{\mathbf{k},\sigma} (t_{\alpha}^{\dagger} c_{\sigma}^{\dagger} a_{\mathbf{k},\sigma}^{\alpha} + t_{\alpha} a_{\mathbf{k},\sigma}^{\alpha\dagger} c_{\sigma}), \quad (2)$$

where t_{α}^{\dagger} and t_{α} are tunneling parameters. We assume symmetric tunneling such that $t_L = t_R$. Since we consider the case that there is no bonding between the molecule and the electrodes, we assume weak coupling of the molecule to the electrodes. Thus, sequential tunneling is dominant. The tunneling parameters may, in general, depend on charge state, magnetic level, magnetic field, or gate voltage. However, we assume that the tunneling parameters are constant, i.e. do not depend on

any of them. It is not the scope of this work to include such dependence or to estimate the values of tunneling parameters.

Considering the weak coupling between the electrodes and the molecule, \mathcal{H}_T is a small perturbation to \mathcal{H}_{el} and \mathcal{H}_{mol} . A total wave function, $|\Psi\rangle$, of $\mathcal{H} = \mathcal{H}_{mol} + \mathcal{H}_{el} + \mathcal{H}_T$ can be expressed as a direct product of a wave function of electrode α and molecular eigenstate $|q\rangle$. As a basis set for \mathcal{H}_{mol} , we use $\{|S = 11/2, M\rangle, M = -11/2, -9/2, \dots, 9/2, 11/2\}$, where M are eigenvalues of the z component of spin operator S_z . The molecular levels in the $N = 0$ state can be written in terms of the basis set and the spinors ($|\uparrow\rangle, |\downarrow\rangle$) by using Clebsch-Gordon coefficients. The molecular eigenstates for state $N = -1$ ($N = 0$) can be written as $\sum_j u_j |M_j\rangle$ ($\sum_k v_k |m_k\rangle$), where u_j (v_k) are coefficients and $M_j = -11/2, \dots, 11/2$ ($m_k = -6, \dots, 6$).

In the sequential tunneling limit, transition rates $R_{i \rightarrow f}$ from initial state $|\Psi_i\rangle$ to final state $|\Psi_f\rangle$, are shown as $2\pi/\hbar |\langle \Psi_f | \mathcal{H}_t | \Psi_i \rangle|^2 \delta(E_f - E_i)$, to the lowest order in \mathcal{H}_T , where E_f and E_i are the final and initial energies, respectively. The transition rates are integrated over \mathbf{k} and thermal distributions of electrons in the electrodes are described by the Fermi-Dirac distribution function $f(E)$. For electron tunneling from electrode α to the molecule, the molecule undergoes a transition from level $|q\rangle$ in the $N = -1$ state to level $|r\rangle$ in the $N = 0$ state, where $|q\rangle = \sum_j u_j |M_j\rangle$ and $|r\rangle = \sum_k v_k |m_k\rangle$. The corresponding transition rates $\gamma_{\alpha}^{q \rightarrow r}$, are given by^{3,24,29,30}

$$\gamma_{\alpha}^{q \rightarrow r} = \sum_{\sigma} W_{q \rightarrow r}^{\sigma, \alpha} f(\epsilon_r - \epsilon_q - \mu_{\alpha}), \quad (3)$$

where $W_{q \rightarrow r}^{\sigma, \alpha}$ is $\frac{2\pi}{\hbar} \mathcal{D}_{\sigma}^{\alpha} |t_{\alpha}|^2 |\langle r | c_{\sigma}^{\dagger} | q \rangle|^2$, and $\mathcal{D}_{\sigma}^{\alpha}$ is density of states of electrode α near the Fermi level (E_F). We assume that $\mathcal{D}_{\sigma}^{\alpha}$ is constant and that it is independent of α and σ . Here μ_{α} is a chemical potential of electrode α . Considering a symmetric bias application, we set $\mu_L = eV/2$ and $\mu_R = -eV/2$, where V is a bias voltage. The matrix elements $\langle r | c_{\sigma}^{\dagger} | q \rangle$ determine selection rules such as $|\Delta S| = 1/2$, $|M_j - m_k| = 1/2$, and $\Delta N = \pm 1$. For tunneling from the molecule to electrode α , the molecule make a transition from $|r\rangle$ to $|q\rangle$. The transition rates are now given by

$$\gamma_{\alpha}^{r \rightarrow q} = \sum_{\sigma} W_{r \rightarrow q}^{\sigma, \alpha} [1 - f(\epsilon_r - \epsilon_q - \mu_{\alpha})], \quad (4)$$

where $[1 - f(\epsilon_r - \epsilon_q - \mu_{\alpha})]$ is included because the final state must be unoccupied for an electron to tunnel back to electrode α .

Probabilities P_q of molecular states $|q\rangle$ being occupied must satisfy the following master equation^{3,24,28-30}

$$\frac{dP_q}{dt} = -P_q \sum_{\alpha=L,R} \sum_r \gamma_{\alpha}^{q \rightarrow r} + \sum_{\alpha=L,R} \sum_r \gamma_{\alpha}^{r \rightarrow q} P_r, \quad (5)$$

where the summation over r runs for the orbital and magnetic degrees of freedom. The first (second) term cov-

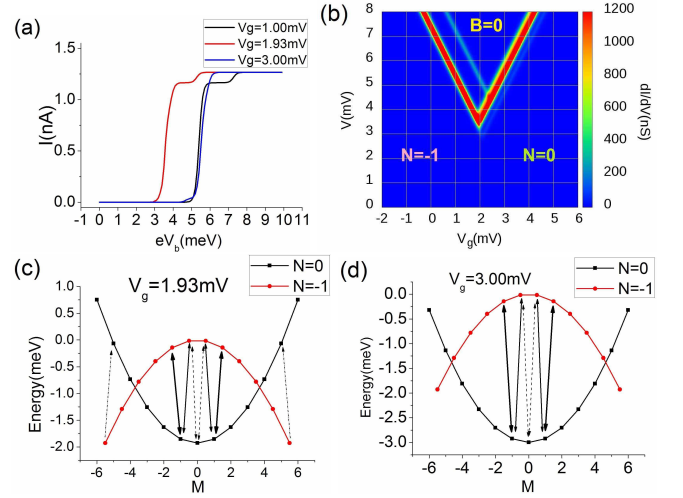


FIG. 2: (Color online) (a) Calculated I - V curves at $V_g = 1.0$, 1.93 , and 3.0 mV for $T=0.05$ meV/ k_B . (b) Calculated dI/dV as a function of V and V_g for $B = 0$. The magnetic levels in the $N=0$ and $N=1$ states for (c) $V_g = 1.93$ mV and (d) $V_g = 3.0$ mV with $B = 0$. Arrows in (c) and (d) indicate transitions where the energy differences between the involved levels are comparable to $eV/2$ for the first dI/dV peak.

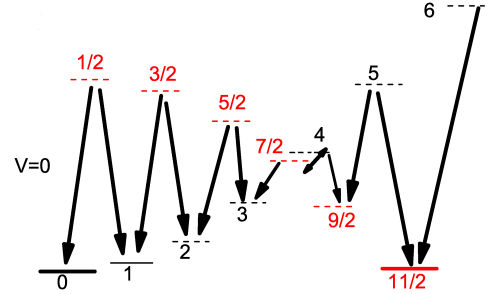


FIG. 3: (Color online) Schematic diagram to elucidate the mechanism for the spin blockade effect at $B = 0$ for $V = 0$ mV and $V_g = 1.93$ mV. Only the m and M levels with $m, M > 0$ are shown since the $m, M < 0$ levels are degenerate with the $m, M > 0$ levels. The thicknesses of the levels represent the values of the level occupation probabilities: thicker lines for higher occupation probabilities. The dashed lines indicate that their occupation probabilities are zero. Thicker arrows show that their transition rates are non-zero. None of the indicated transitions contribute to the current at zero bias. See the text for details.

ers all allowed transitions from (to) $|q\rangle$. To find steady-state probabilities, we solve $dP_q/dt = 0$ for P_q , by applying the bi-conjugate gradient stabilized algorithm³¹ with the zero-bias Boltzmann distribution as initial occupation probabilities. Then the current from electrode α to the molecule is computed from

$$I_{\alpha=L,R} = e \sum_{q,r} \gamma_{\alpha}^{[N=-1,q] \rightarrow [N=0,r]} P_q - e \sum_{q,r} \gamma_{\alpha}^{[N=0,r] \rightarrow [N=-1,q]} P_r, \quad (6)$$

where the sums over q and r run for all orbital and magnetic indices. The total current is obtained from $I = (I_L - I_R)/2$. A differential conductance (dI/dV) is numerically calculated from current-voltage ($I-V$) characteristics by using a small bias interval $\Delta V \leq 0.1$ mV.

III. RESULTS AND DISCUSSION

We present calculated dI/dV as a function of V and V_g at temperature $T = 0.58$ K (or 0.05 meV/ k_B) for $\mathbf{B} = 0$ and for \mathbf{B} field along the z axis and the x axis, separately. In all cases, the level broadening parameter, $\Gamma = 2\pi\mathcal{D}|t|^2$, is set to be 0.01 meV such that $\Gamma \ll k_B T$, where \mathcal{D} is density of states of the electrodes and k_B is the Boltzmann constant. Only sequential tunneling is considered since it is dominant. Our work qualitatively differs from the previous work on the molecule³² because the magnetic levels were not considered in the latter.

A. Spin blockade without B field

Figure 2(a) shows our calculated $I-V$ curves at three gate voltages for $\mathbf{B} = 0$. At $V_g = 1.93$ mV current flows through the molecule only for $V \geq 3.4$ mV, and it increases further near 5.4 mV with a small step. At $V_g = 1.0$ and 3.0 mV current flows for $V \geq 5.3$ mV. In the three cases current is blocked until V reaches a certain value. The same feature is found at any other gate voltages, as shown in Fig. 2(b). This current suppression at low bias is the essence of our work, i.e. the magnetic-anisotropy induced spin blockade effect.

With $V_g = 1.93$ mV the molecule is at the charge degeneracy point (CDP), where the lowest levels in the two charge states, $|N = -1; S = 11/2, M = \pm 11/2\rangle$ and $|N = 0; S = 6, m = 0\rangle$, are degenerate as shown in Fig. 2(c). At $V = 0$, in the $N = -1$ state only the $M = \pm 11/2$ levels are occupied with probabilities of 29 and 29%, while in the $N = 0$ state the $m = 0$ and $m = \pm 1$ levels have occupation probabilities of 29, 6.5, and 6.5%, respectively. The rest of the levels are not occupied because there are zero rates of transitions from the occupied levels to higher-energy levels, although the transitions are allowed by the selection rules. (Only rates of the reverse transitions are quite high.) See Fig. 3]. The former transition rates vanish since there are no occupied electrons at the corresponding energy levels in the electrodes according to the Fermi-Dirac distribution $f(E)$. Furthermore, there are no allowed transitions among the occupied levels. Therefore, no current flows at zero bias. Increasing the bias, some higher levels enter the bias window. Due to the symmetric bias application, only the levels whose energy differences are less than about $eV/2$ can contribute to the current. For example, at $V = 2.3$ mV, energy $eV/2$ is close to the energy difference between $M = \pm 5/2$ and $m = \pm 2$ [Figs. 2(c) and 3]. Thus, at $V = 2.3$ mV, transitions such as ($|M = \pm 7/2\rangle$,

$|m = \pm 3\rangle$), ($|m = \pm 4\rangle$, $|M = \pm 7/2\rangle$), ($|m = \pm 4\rangle$, $|M = \pm 9/2\rangle$), and ($|M = \pm 5/2\rangle$, $|m = \pm 2\rangle$), are allowed by the selection rules and possible in terms of energy differences. However, higher energy levels $m = \pm 2, \pm 3, \pm 4$ and $M = \pm 5/2, \pm 7/2, \pm 9/2$ are not occupied since there are no transition pathways to occupy them from the zero-bias occupied levels at this bias voltage. Therefore, these higher levels cannot contribute to the current. Only when there exist significant transition rates *from* at least one of the initial (zero-bias) five occupied levels $M = \pm 11/2$ and $m = 0, \pm 1$ to higher levels, the higher-energy levels are occupied. Then the occupied levels can contribute to the current and they induce other transitions. Figure 4(a) shows occupation probabilities, transition rates, and percentage contributions to the current at $V = 3.4$ mV for the positive m and M levels including $m = 0$. Note that the negative m and M levels are degenerate with the positive m and M levels. At this bias, the energy differences between $m = \pm 1$ and $M = \pm 1/2$ or $M = \pm 3/2$ are comparable to $eV/2$. All m levels except for $m = \pm 6$ and all M levels are within the bias window. Significant transition rates from $m = \pm 1$ to $M = \pm 3/2$ make the $M = \pm 3/2$ level occupied. This triggers subsequent transitions such as $|M = \pm 3/2\rangle \leftrightarrow |m = \pm 2\rangle \leftrightarrow |M = \pm 5/2\rangle \leftrightarrow |m = \pm 3\rangle \leftrightarrow |M = \pm 7/2\rangle \leftrightarrow |m = \pm 4\rangle \leftrightarrow |M = \pm 9/2\rangle \leftrightarrow |m = \pm 5\rangle$, as shown in Fig. 4(a). There exist also small transition rates from $M = \pm 11/2$ to $m = \pm 5$. All of these transitions enable all m levels except for $m = \pm 6$ and all M levels to be occupied to some extent. Therefore, these transitions can contribute to the large step near $V = 3.4$ mV in the $I-V$ curve [Fig. 2(a)]. When the bias increases slightly more like $V = 3.68$ mV, transitions from $m = 0$ to $M = \pm 1/2$ increase, which makes transitions such as ($|M = \pm 1/2\rangle$, $|m = 1\rangle$) and ($|m = \pm 5\rangle$, $|M = \pm 11/2\rangle$) additionally contribute to the current. Now the small second step near $V = 5.4$ mV in the $I-V$ plot can be explained by allowed transitions from $M = \pm 11/2$ to $m = \pm 6$, where the energy difference between the levels is 2.68 meV.

At $V_g = 1.0$ mV the molecule is in the cationic state (at $|S = 11/2, M = \pm 11/2\rangle$) for zero bias. The energy levels at this gate voltage are shown in Fig. 4(b). In this case, high current is expected only above $V = 5.3$ mV because there are no transition pathways from the zero-bias occupied levels ($M = \pm 11/2$) to allowed levels in state $N = 0$ at bias below $V = 5.3$ mV. At $V = 5.4$ mV, there are small rates of transitions from $M = \pm 11/2$ to $m = \pm 5$, and all M and m levels except for $m = \pm 6$ are within the bias window. See Figs. 2(a) and 4(b). Thus, these transitions induce a series of transitions such as $|m = \pm 5\rangle \leftrightarrow |M = \pm 9/2\rangle \leftrightarrow |m = \pm 4\rangle \leftrightarrow |M = \pm 7/2\rangle \leftrightarrow |m = \pm 3\rangle \leftrightarrow |M = \pm 5/2\rangle \leftrightarrow |m = \pm 2\rangle \leftrightarrow |M = \pm 3/2\rangle \leftrightarrow |m = \pm 1\rangle \leftrightarrow |M = \pm 1/2\rangle \leftrightarrow |m = 0\rangle$. As a result, the levels within the bias window are all occupied with some probabilities. Therefore, these levels contribute to the high current. The second small step in the $I-V$ curve is caused by the transitions from $M = \pm 11/2$ to $m = \pm 6$, similarly to the case of $V_g = 1.93$ mV,.

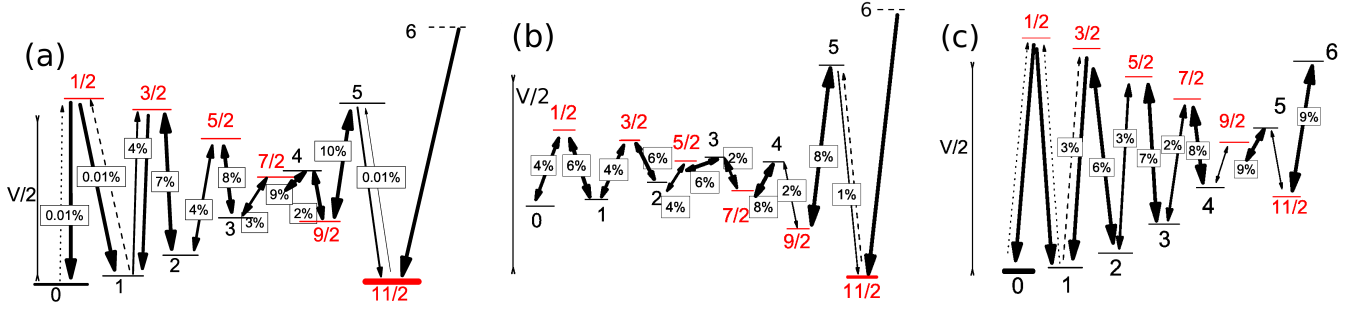


FIG. 4: (Color online) Schematic diagrams to elucidate the mechanism for the lifting of the spin blockade effect at $B = 0$ for (a) $V = 3.4$ mV and $V_g = 1.93$ mV, (b) $V = 5.4$ mV and $V_g = 1.0$ mV, and (c) $V = 5.4$ mV and $V_g = 3.0$ mV. Only the m and M levels with $m, M > 0$ are shown. The thicknesses of the levels represent the values of the occupation probabilities: thicker lines for higher occupation probabilities. The dashed horizontal lines indicate that the occupation probabilities are zero. Thicker arrows are for higher transition rates and dashed arrows are for smallest transition rates. Only non-zero transition rates are shown. Boxed numbers indicate percentage contributions of particular transition pathways to the current. For transitions which do not contribute to the current, boxed numbers are absent. The bias window is shown.

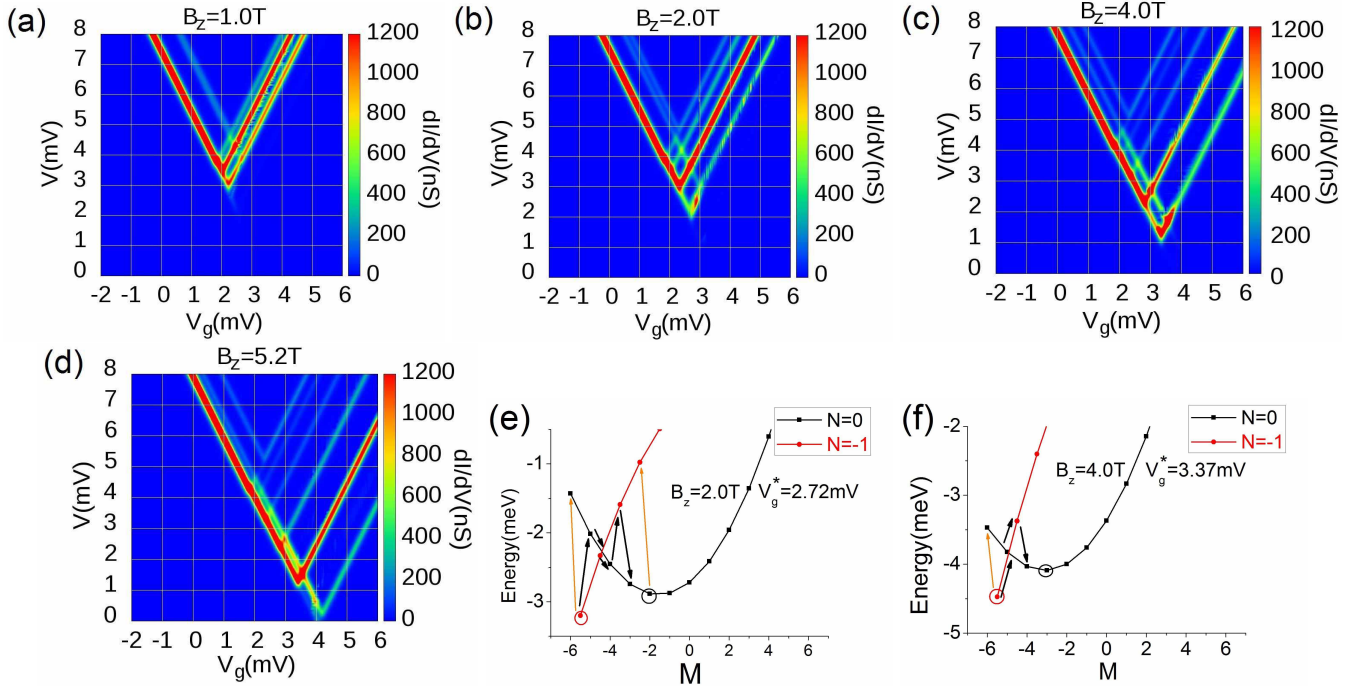


FIG. 5: (Color online) (a)-(d) Calculated dI/dV values as a function of V and V_g at $T = 0.05$ meV/ k_B for several B_z values. Magnetic level energies in the two charge states (e) for $B_z = 2.0$ T at $V_g^* = 2.72$ mV and for (f) $B_z = 4.0$ T at $V_g^* = 3.37$ mV. Not all the levels are shown in (e) and (f). The thick black (thin red) arrows in (e) and (f) indicate allowed transitions for the first (second) dI/dV peak and the circled levels are the lowest levels for the $N = -1$ and $N = 0$ states. See the text for details.

Now at $V_g = 3.0$ mV the molecule is in the neutral state with probabilities of 68.8, 15.6, and 15.6% at the $m = 0$ and $m = \pm 1$ levels, respectively, at zero bias. The energy levels at this gate voltage are shown in Fig. 4(c). In this case, only one giant step appears in current near $V = 5.3$ mV [Fig. 2(a) and (d)] since there are no transition pathways from the zero-bias occupied levels ($m = 0$ and $m = \pm 1$) to allowed levels in state $N = -1$ at bias below $V = 5.3$ mV. At $V = 5.4$ mV, the energy differences between $m = \pm 1$ and $M = \pm 3/2$ are comparable to

$eV/2$. All m and M levels are within the bias window (levels $M = \pm 1/2$ are only slightly outside the window), as shown in Fig. 4(c). Thus, the transitions from $m = \pm 1$ to $M = \pm 3/2$ occur with significant rates, which gives some occupation probabilities at the $M = \pm 3/2$ levels. Then this induces a series of transitions similar to the case of $V_g = 1.93$ and $V = 3.4$ mV, and now the transitions between $M = \pm 11/2$ and $m = \pm 6$ also occur because the energy difference between the levels is much smaller due to the increased gate voltage. Compare

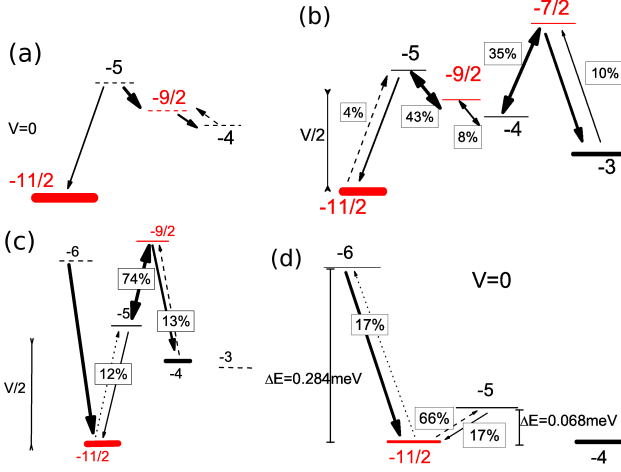


FIG. 6: (Color online) Schematic diagrams to elucidate the mechanisms for the spin blockade effect and for the lifting of the effect at $B_z = 2.0$ T and $V_g^* = 2.72$ mV for (a) $V = 0$ and (b) $V = 2.0$ mV, and (c) at $B_z = 4.0$ T for $V_g = 3.37$ mV and $V = 1.0$ mV and (d) at $B_z = 5.2$ T for $V_g = 4.02$ mV and $V = 0$. The energy levels in (a) and (b) are zoom-in of Fig. 5(e), while the energy levels in (c) are zoom-in of Fig. 5(f). Only relevant levels in the $N = -1$ (red) and $N = 0$ (black) states are shown. The levels not shown have extremely small or zero occupation probabilities or not relevant to our discussion. The thicknesses of the levels represent the values of the occupation probabilities: thicker lines for higher occupation probabilities. The dashed horizontal lines indicate that the occupation probabilities are zero. Thicker arrows are for higher transition rates and dashed arrows are for smallest transition rates. Only non-zero transition rates are shown. Boxed numbers indicate percentage contributions of particular transition pathways to the current. The bias window is shown. The vertical energy scales in (a) and (b) are the same, but they differ from those in (c) and (d).

Fig. 4(a) to 4(c). There are small transition rates from $m = 0$ to $M = \pm 1/2$. All m and M levels are occupied to some extent. Therefore, high current is expected near $V = 5.3$ mV. Our analysis of the I - V curves at the three different gate voltages clearly reveals that the blockade effect at low bias cannot be lifted by gate voltage.

B. In the presence of B_z field

Figure 5(a)-(d) shows calculated dI/dV as a function of V and V_g at several \mathbf{B} fields when the field is applied along the z axis. As B_z increases, the spin blockade region becomes narrower and the tip of the V-shaped dI/dV peak shifts toward higher gate voltage. This blockade effect persists until B_z reaches about 5.2 T at $T = 0.05$ meV/ k_B . With increasing B_z (> 0), the energies of the $M, m < 0$ levels become lower, while those of the $M, m > 0$ levels higher, due to the Zeeman energy [Fig. 5(e),(f)]. This level shift modifies the transition rates Eqs. (3) and (4) and the occupation probabilities

$P_{q,r}$ of the levels at given bias and gate voltages. Note that in our model and Fig. 5 (a)-(d), the tunneling parameters are kept independent of charge state, magnetic level, magnetic field, or gate voltage. Equations (3) and (4) indicate that such a dependence of the tunneling parameters would change the transition rates and so it leads to changes in the heights of dI/dV peaks, but these changes would occur only for transitions allowed by the selection rules and the Fermi-Dirac distribution $f(E)$ within the bias window. Therefore, this dependence would not eliminate the blockade effect at zero or low bias. For $B_z > 0$ the lowest level in the cationic state is always $M = -11/2$, whereas the lowest level $-m$ ($m > 0$) in the neutral state changes with B_z . From the energy eigenvalues, we find that this m value is given by a round-off integer of $g\mu_B B_z / (2|D_0|)$, in agreement with our numerical calculation.

As shown in Fig. 5(b) and (e), at $B_z = 2.0$ T, the lowest level in the $N = 0$ state is $m = -2$, and the current starts to flow at $V = 2.0$ mV for $V_g^* = 2.72$ mV. For any other gate voltage, higher bias than 2.0 mV is needed for current to flow. The threshold bias is much lower than that at zero magnetic field, i.e. 3.4 mV. At $V_g^* = 2.72$ mV the molecule is in the cationic state since the $M = -11/2$ level has a lower energy than the $m = -2$ level. At zero bias, only the $M = -11/2$ level is occupied and the transition rate from $M = -11/2$ to $m = -5$ is zero despite a significant rate of the reverse transition, as shown in Fig. 6(a). The former transition rate vanishes because of zero occupied electrons at the corresponding energy in the electrodes according to the Fermi-Dirac distribution function. As bias increases to $V = 2.0$ mV [Figs. 6(b) and 5(e)], the levels $M = -11/2, -9/2$ and $m = -4, -3, -2, -1, 0, 1$ enter the bias window and the levels $m = -5, 2$ are slightly outside the bias window. There exists some transition rate from $M = -11/2$ to $m = -5$, which makes the $m = -5$ level occupied. This triggers ensuing transitions such as $|m = -5\rangle \leftrightarrow |M = -9/2\rangle \leftrightarrow |m = -4\rangle$ [Figs. 6(b) and 5(e)]. These transitions induce significant occupation probabilities at levels $m = -5, -4$ and $M = -9/2$. Then the $M = -7/2$ level is now within the bias window with respect to the $m = -4$ level, and a transition between $m = -4$ and $M = -7/2$ is now allowed. This gives rise to a substantial occupation probability at the $M = -7/2$ level. Then a transition between $M = -7/2$ and $m = -3$ is also allowed within the bias window, producing a high occupation probability at the $m = -3$ level. This whole process contributes to the high current at $V = 2.0$ mV. The key step to lift the spin blockade effect is to produce a substantial occupation probability at the $m = -5$ level via a sizeable transition rate to the $m = -5$ level from the zero-bias occupied level, $M = -11/2$. As bias increases further to 3.7 mV, the bias window additionally includes the $m = -6$ level. Then there is a substantial rate of transition from $M = -11/2$ to $m = -6$ and the transition rate from $M = -11/2$ to $m = -5$ increases. The increased transition rates trigger transitions similar

to the lower-bias case. With respect to the $m = -3$ level, now the $M = -5/2$ level enters the bias window. Thus, there exist a transition between $M = -5/2$ and $m = -3$, and consequently the $M = -5/2$ level is occupied. A transition from $M = -5/2$ to $m = -2$ now makes the $m = -2$ level occupied, and its reverse transition is also possible. All of these transitions contribute to the strong dI/dV peak near $V = 3.7$ mV, as shown in Fig. 5(b) and (e). The V_g^* value differs from the CDP, $V_g = 3.03$ mV.

When B_z reaches 4.0 T, $m = -3$ is the lowest level in the $N = 0$ state, and the current begins to flow at $V = 1.0$ mV for $V_g^* = 3.37$ mV [Fig. 5(c) and (f)]. The threshold bias is much more reduced than the case of $B_z = 2.0$ T. At $V_g^* = 3.37$ mV the molecule is in the cationic state. At zero bias, only the $M = -11/2$ level is occupied and the transition rate from $M = -11/2$ to $m = -5$ vanishes despite a significant rate of the reverse transition, due to the same reason as in the case of $B_z = 2.0$ T. Thus, the $m = -5$ level is unoccupied and current cannot flow. For $V = 1.0$ mV, the transition from $M = -11/2$ to $m = -5$ occurs and so the $m = -5$ level is occupied [Fig. 6(c)]. Then the $M = -9/2$ level is within the bias window with respect to the $m = -5$ level. Since the transition rate from $m = -5$ to $M = -9/2$ is significant, the $M = -9/2$ level is occupied. As a result, the transition between $M = 9/2$ and $m = -4$ occurs. There are high occupation probabilities at the $M = -11/2$ and $m = -4$ levels. These series of transitions $|M = -11/2\rangle \leftrightarrow |m = -5\rangle \leftrightarrow |M = -9/2\rangle \leftrightarrow |m = -4\rangle$ contribute to the high current, as indicated with thick arrows in Fig. 5(f). The largest contribution to the current arises from the transition between $m = -5$ and $M = -9/2$.

As B_z increases even further, the $m = -5$ level becomes the lowest in the $N = 0$ state. This occurs at $B_z^* = 5.78$ T based on $4.5 = g\mu_B B_z / (2|D_0|)$. Then at the CDP V_g where the $M = -11/2$ and $m = -5$ levels are degenerate, the spin blockade is lifted. However, B_z^* is slightly higher than the threshold field (~ 5.2 T) obtained from our calculated stability diagrams [Fig. 5(d)]. This difference can be explained by thermal broadening. At $B_z = 5.2$ T the lowest level in the $N = 0$ state is $m = -4$ and the corresponding CDP is 4.02 mV. At this CDP, the energy difference between $M = -11/2$ and $m = -5$ is about 0.068 meV [Fig. 6(d)]. Considering the thermal energy ($k_B T = 0.05$ meV), the $m = -5$ level has some occupancy even at $V = 0$. Thus, most of the current at zero bias arises from the transition between $M = -11/2$ and $m = -5$. Note that in this case the magnitude of the zero-bias current is one order of magnitude smaller than the magnitude of the current at the first dI/dV peak for lower B_z fields.

We also examine the dependence of the threshold B_z field on D_0 and D_{-1} . We find that the threshold field depends only on D_0 , as long as the zero-field splitting determined by D_{-1} is greater than the thermal energy. The threshold B_z field linearly increases with increasing $|D_0|$.

C. In the presence of B_x field

Figure 7(a) and (b) shows calculated stability diagrams when \mathbf{B} is along the x axis. As B_x increases, the spin blockade region becomes narrower and the tip of the V-shaped dI/dV peak shifts toward lower gate voltage. Similarly to the case of the B_z field, the spin blockade effect is still observed until B_x increases to about 3.0 T at $T = 0.05$ meV/ k_B . The threshold B_x field is lower than the threshold B_z field. With B_x the molecular eigenstates for each charge state are linear combinations of different M (or m) levels. For example, Fig. 7(c) shows eleven lowest energy levels at $B_x = 1.0$ T for the CDP $V_g = 1.40$ mV. The lowest level for $N = 0$ (state 1) is $-0.07|m = -3\rangle + 0.23|m = -2\rangle - 0.49|m = -1\rangle + 0.63|m = 0\rangle - 0.49|m = 1\rangle + 0.23|m = 2\rangle - 0.07|m = 3\rangle$, while the two lowest levels for $N = -1$ (states 2 and 3) are $0.68|M = -11/2\rangle - 0.20|M = -9/2\rangle + 0.05|M = -7/2\rangle \mp 0.05|M = 7/2\rangle \pm 0.20|M = 9/2\rangle \mp 0.68|M = 11/2\rangle$. At zero bias, the selection rules allow transitions between state 1 and state 2 or 3 due to small contributions of $|m = \pm 3\rangle$ to state 1 and of $|M = \pm 7/2\rangle$ to states 2 and 3. However, their contributions to the current are negligible at zero bias because of the small coefficients in the eigenstates. There are no other contributions to the current at zero bias. As V increases, higher levels are accessible and occupied. At $V = 1.10$ mV, the excited level, state 4, for $N = 0$, has substantial contributions from $|m = \pm 3\rangle$ and small additional contributions from $|m = \pm 4\rangle$, while the excited levels for $N = -1$ (states 5 and 6) have large contributions from $M = \pm 7/2$ and substantial (small) additional contributions from $M = \pm 5/2$ ($M = \pm 3/2$). This gives rise to a sizeable rate of transition from state 3 to state 4, which makes state 4 occupied [Fig. 7(c)]. Then there occur a series of transitions such as [state 4] \leftrightarrow [state 6] \leftrightarrow [state 8] \leftrightarrow [state 10], within the bias window. Furthermore, there exists a small rate of transition from state 1 to state 5, which makes state 5 occupied. This leads to two kinds of transition pathways such as [state 5] \leftrightarrow [state 7] \leftrightarrow [state 9] and [state 5] \leftrightarrow [state 11] among the eleven lowest energy levels. All of these transitions contribute to the current at $V = 1.10$ mV [Fig. 7(a) and (c)]. As B_x further increases to 3.0 T, the lowest level in each charge state has contributions from all M or m levels, which allows current at zero bias [Fig. 7(b)]. We find that the threshold B_x field depends only on D_{-1} , and it decreases as $|D_{-1}|$ decreases.

IV. CONCLUSION

We have examined the electron transport properties of the $\text{Eu}_2(\text{COT})_3$ molecule weakly coupled to the non-magnetic electrodes in the sequential tunneling limit. Our calculated dI/dV peaks as a function of V and V_g showed that the current is strongly suppressed at low bias independently of V_g due to the interplay between the sign reversal of magnetic anisotropy parameter D_N and

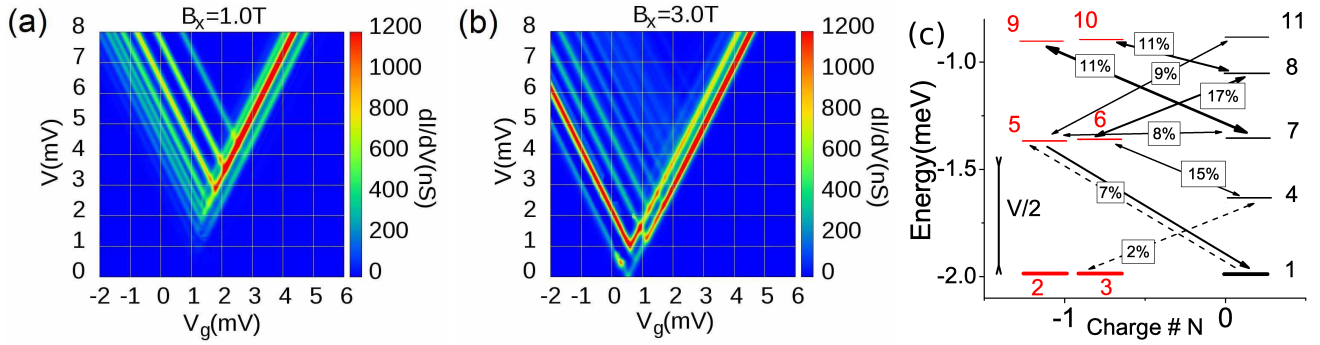


FIG. 7: (Color online) Calculated dI/dV as a function of V and V_g for (a) $B_x = 1.0$ and (b) 3.0 T at $T = 0.05$ meV/ k_B . (c) Calculated eleven lowest energy levels in the $N = -1$ and $N = 0$ states for $B_x = 1.0$ T at $V_g = 1.40$ mV with their occupation probabilities, transition rates, and percentage current contributions to the first dI/dV peak at $V = 1.1$ mV. Lines, arrows, and boxed numbers have the same meanings as those in Fig. 6. Levels 1, 4, 7, 8, and 11 are for $N = 0$, and the rest of the levels are for $N = -1$. Here only transition rates contributing to significant current are shown.

the selection rules for the occupied levels. The threshold B_z (B_x) field depends only on the easy-plane (easy-axis) magnetic anisotropy parameter.

Acknowledgments

The authors were supported by the U. S. National Science Foundation DMR-1206354.

-
- * Electronic address: luogp12@vt.edu; Electronic address: kyungwha@vt.edu
- ¹ S. Thiele, F. Balestro, R. Ballou, S. Klyatskaya, M. Ruben, and W. Wernsdorfer, *Science* **344**, 1135 (2014).
 - ² M. N. Leuenberger and E. R. Mucciolo, *Phys. Rev. Lett.* **97**, 126601 (2006).
 - ³ M. Misiorny and J. Barnaś, *Phys. Rev. B* **76**, 054448 (2007).
 - ⁴ A. A. Khajetoorians, B. Baxevanis, C. Hubner, T. Schlenk, S. Krause, T. O. Wehling, S. Lounis, A. Lichtenstein, D. Pfannkuche, J. Wiebe, and R. Wiesendanger, *Science* **339**, 55 (2013).
 - ⁵ H. B. Heersche, Z. de Groot, J. A. Folk, H. S. van der Zant, C. Romeike, M. R. Wegewijs, L. Zobbi, D. Barreca, E. Tondello, and A. Cornia, *Phys. Rev. Lett.* **96**, 206801 (2006).
 - ⁶ S. Barraza-Lopez, K. Park, V. García-Suárez, and J. Ferrer, *Phys. Rev. Lett.* **102**, 246801 (2009).
 - ⁷ Y.-N. Wu, X.-G. Zhang, and H.-P. Cheng, *Phys. Rev. Lett.* **110**, 217205 (2013).
 - ⁸ K. Park and M. R. Pederson, *Phys. Rev. B* **70**, 054414 (2004).
 - ⁹ A. S. Zyazin, J. W. G. van den Berg, E. A. Osorio, H. S. J. van der Zant, N. P. Konstantinidis, M. Leijnse, M. R. Wegewijs, F. May, W. Hofstetter, C. Danieli, and A. Cornia, *Nano Lett.* **10**, 3307-3311 (2010).
 - ¹⁰ Z. Zhang, X. Wu, W. Guo, and X. C. Zeng, *J. Am. Chem. Soc.* **132**, 10215 (2010).
 - ¹¹ K. Park and J.-Z. Wang, *Polyhedron* **66**, 157 (2013).
 - ¹² X.-G. Li, J. N. Fry, and H.-P. Cheng, *Phys. Rev. B* **90**, 125447 (2014).
 - ¹³ N. Atodiressei, P. H. Dederichs, Y. Mokrousov, L. Bergqvist, G. Bihlmayer, S. Blügel, *Phys. Rev. Lett.* **100**, 117207 (2008).
 - ¹⁴ P. Gambardella, S. Stepanow, A. Dmitriev, J. Honolka, F. M. F. de Groot, M. Lingenfelder, S. S. Gupta, D. D. Sarma, P. Bencok, S. Stanescu, S. Clair, S. Pons, N. Lin, A. P. Seitsonen, H. Brune, J. V. Barth, and K. Kern, *Nat. Mat.* **8**, 189 (2009).
 - ¹⁵ H. Yang, A. D. Vu, A. Hallal, N. Rougemaille, J. Coraux, G. Cheng, A. K. Schmid, and M. Chshiev, *Nano Lett.* **16**, 145 (2016).
 - ¹⁶ K. Miyajima, T. Kurikawa, M. Hashimoto, and A. Nakajima, *Chem. Phys. Lett.* **306**, 256 (1999).
 - ¹⁷ N. Hosoya, R. Takegami, J. Suzumura, K. Yada, K. Koyasu, K. Miyajima, M. Mitsui, M. B. Knickelbein, S. Yabushita, and A. Nakajima, *J. Phys. Chem. A* **109**, 9 (2005).
 - ¹⁸ F. T. Edelmann, *N. J. Chem.* **35**, 517 (2011).
 - ¹⁹ J. J. Le Roy, M. Jeletic, S. I. Gorelsky, I. Korobkov, L. Ungur, L. F. Chibotaru, and M. Murugesu, *J. Am. Chem. Soc.* **135**, 3502 (2013).
 - ²⁰ T. Tsuji, N. Hosoya, S. Fukazawa, R. Sugiyama, T. Iwasa, H. Tsunoyama, H. Hamaki, N. Tokitoh, and A. Nakajima,

- J. Phys. Chem. C **118**, 5896 (2014).
- ²¹ D. Weinmann, W. Häusler, and B. Kramer, Phys. Rev. Lett. **74**, 984 (1995).
 - ²² K. Ono, D. G. Austing, Y. Tokura, and S. Tarucha, Science **297**, 1313 (2002).
 - ²³ A. C. Johnson, J. R. Petta, C. M. Marcus, M. P. Hanson, and A. C. Gossard, Phys. Rev. B **72**, 165308 (2005).
 - ²⁴ J. Koch and F. von Oppen, Phys. Rev. Lett. **94**, 206804 (2005).
 - ²⁵ E. Burzuri, Y. Yamamoto, M. Warnock, X. Zhong, K. Park, A. Cornia, and H. S. J. van der Zant, Nano Lett. **14**, 3191 (2014).
 - ²⁶ E. Burzuri, A. Zyazin, A. Cornia, and H. S. J. van der Zant, Phys. Rev. Lett. **109**, 147203 (2012).
 - ²⁷ M. H. Jo, J. E. Grose, J. Baheti, M. M. Deshmukh, J. J. Sokol, E. M. Rumberger, D. N. Hendrickson, J. R. Long, H. Park, and D. C. Ralph, Nano Lett. **6**, 2014 (2006).
 - ²⁸ A. McCaskey, Y. Yamamoto, M. Warnock, E. Burzuri, H. S. J. van der Zant, and K. Park, Phys. Rev. B **91**, 125419 (2015).
 - ²⁹ M. Misiorny, I. Weymann, and J. Barnas, Europhys. Lett. **89**, 18003 (2010).
 - ³⁰ M. Misiorny, I. Weymann, and J. Barnas, Phys. Rev. B **79**, 224420 (2009).
 - ³¹ G. L. Sleijpen and D. R. Fokkema, Elec. Trans. Num. Anal., **1**, 2000 (1993).
 - ³² K. Xu, J. Huang, S. Lei, H. Su, F. Y. C. Boey, Q. Li, and J. Yang, J. Chem. Phys. **131**, 104704 (2009).